

# Rare fluctuations and large-scale circulation cessations in turbulent convection

Michael Assaf<sup>1</sup>, Luiza Angheluta<sup>1,2</sup> and Nigel Goldenfeld<sup>1</sup>

<sup>1</sup>*Department of Physics, University of Illinois at Urbana-Champaign,*

*Loomis Laboratory of Physics, 1110 West Green Street, Urbana, Illinois, 61801-3080*

<sup>2</sup>*Physics of Geological Processes, Department of Physics, University of Oslo, Norway*

In turbulent Rayleigh-Benard convection, a large-scale circulation (LSC) develops in a nearly vertical plane, and is maintained by rising and falling plumes detaching from the unstable thermal boundary layers. Rare but large fluctuations in the LSC amplitude can lead to extinction of the LSC (a cessation event), followed by the re-emergence of another LSC with a different (random) azimuthal orientation. We extend previous models of the LSC dynamics to include momentum and thermal diffusion in the azimuthal plane, and calculate the tails of the probability distributions of both the amplitude and azimuthal angle. Our analytical results are in very good agreement with experimental data.

PACS numbers: 05.65.+b,47.27.eb,47.27.te

When a fluid is heated from below in the presence of a gravitational field, the static state with thermal conduction can become unstable towards a succession of instabilities, ultimately leading to turbulence if the buoyancy-induced driving force is sufficiently greater than the viscous drag and diffusion of heat. This balance is quantified by the Rayleigh number  $Ra = \alpha_0 g \Delta T L^3 / \nu \kappa$ , where  $\alpha_0$  is the isobaric thermal expansion coefficient,  $g$  is the gravity field,  $\Delta T$  is the temperature gap between bottom and top layers,  $L$  is the height of the fluid container,  $\kappa$  is the thermal diffusivity and  $\nu$  is the kinematic viscosity. For large  $Ra$ , thermal boundary layers become unstable by emitting hot (on the bottom) or cold (on the top) plumes which, due to buoyancy, migrate upwards (hot) or downwards (cold) [1–3]. In addition to their vertical motion, plumes drift along the top and bottom boundaries in opposite directions, contributing to a large-scale circulation (LSC) flowing in a nearly vertical plane, which spans the diameter of the container. The horizontal velocity of the plumes oscillates rapidly compared to the reorientation dynamics of the large-scale circulation [4–6], which, in a cylindrical geometry, undergoes both rotational diffusion and orientational jumps following irregular cessation of the entire flow [4, 7]. Such laboratory experiments provide a well-controlled setting in which to study the statistical properties of cessation, reversal and reorientation events similar to those that occur in many flows of practical significance, including atmospheric [8] and oceanic circulation [9], the dynamo driving planetary magnetic fields [10], and in the cores of stars [11].

In order to interpret high quality data on the statistics of cessations and azimuthal rotation, a nonlinear stochastic model that retains physically relevant aspects of the Navier-Stokes equations was developed and shown to reproduce many aspects of the statistics of the azimuthal dynamics and the temperature fluctuations in the LSC plane [12, 13]. The stochastic variables in the model are the amplitude of azimuthal temperature variations,  $\delta$ , induced by the LSC and the azimuthal orientation angle,

$\theta_0$ , of the nearly vertical LSC plane. Although the model predictions are in good agreement with the experimental results for typical fluctuations of the system [13], the model does not account quantitatively for the rare large fluctuations responsible for the cessation statistics and for the broad-tail probability distribution function (PDF) of the azimuthal velocities.

The purpose of this Letter is to extend the stochastic model to capture the tail of the PDFs of the temperature amplitudes and azimuthal velocities. We make three contributions here. Firstly, we show that the equation for the amplitude  $\delta$  needs to explicitly include a constant term, known to scale as  $Ra^{5/4}$ . Such a term was already proposed in Ref. [13] as arising from boundary layer thermal diffusion, but its significance for the asymptotics of the PDF had not been emphasized. Secondly, we show that the description of the azimuthal velocities needs to include viscous diffusion in the boundary layer near the wall. Such a term is generally small compared to the other terms in the equation of motion for  $\theta_0$ , but becomes the dominant contribution when the amplitude  $\delta$  is small, as in a cessation event. Thirdly, we compute the PDFs for both  $\delta$  and  $\theta_0$ , predicting respectively an exponential dependence at small  $\delta$  and a power law of  $-4$  for the large angular velocity asymptotics of  $\theta_0$ . A careful analysis of the experimental data is in very good agreement with these predictions.

*Evolution equation for the LSC amplitude:-* For completeness, we briefly summarize the derivation of the physical model for LSC fluctuations, largely following Refs. [12, 13], but with minor differences noted below. The LSC amplitude evolution is derived from the equation satisfied by the velocity component in the LSC plane,  $u_\phi$ , where only the buoyancy and diffusion terms are retained. Here,  $\phi$  is the angle in the vertical circulation plane of the LSC. The turbulent advection term is discarded on the basis that the convection due to azimuthal motion is small relative to the other terms and the self-advection is replaced by random fluctuations. A spatial

average in a direction perpendicular to the main axis of the cylinder (radial average) is performed. The buoyancy term acts everywhere in the LSC plane, hence the average keeps the same form. On the other hand, momentum diffusion is assumed to dominate only in the viscous boundary layer, so that the average of this term gives a prefactor  $\lambda/L$ , where  $\lambda$  is the viscous boundary layer thickness. The viscous layer thickness can be estimated on dimensional grounds as the length scale where the convective forces balance out the diffusive forces, giving  $U^2/L \simeq \nu U/\lambda^2$ , where  $U(t)$  is the maximum speed just within the viscous boundary layer, and thus is an estimate for the typical turnover velocity of an eddy spanning the LSC-plane. Hence  $\lambda(t) \sim \sqrt{\nu L/U}$  and the spatial average of the diffusion term is estimated as  $\langle \nu \nabla^2 u_\phi \rangle \simeq -\nu U/(L\lambda) \simeq -\nu^{1/2} U^{3/2}/L^{3/2}$ . Furthermore, we assume that the amplitude of azimuthal temperature variation,  $\delta$ , is proportional to the large-scale typical velocity of thermal convection rolls  $U$ , in the approximation that momentum acceleration is due to buoyancy forces; this proportionality argument is different from one used in Ref. [13], where buoyancy is balanced against diffusion. Finally, a delta-correlated Gaussian stochastic forcing  $f_\delta(t)$  with amplitude  $D_\delta$  is included to simulate the effect of turbulent fluctuations. As noted in Ref. [13], the resulting equation incorrectly accounts for the small  $\delta$  behavior, where the thermal boundary layer cannot be neglected. Thermal diffusion leads to a constant driving term  $\dot{\delta} = A$  empirically [7] found to scale as  $\text{Ra}^{5/4}$ . This has the effect of driving the system back to the vicinity of  $\delta = \delta_0$ , where the mean LSC amplitude is denoted by  $\delta_0 \approx \Delta T \sigma \text{Re}^{3/2}/\text{Ra}$  and  $\sigma = \nu/\kappa$  is the Prandtl number. By rescaling time  $t \rightarrow t/\tau_\delta$ , where  $\tau_\delta \approx L^2/(\nu \text{Re}^{1/2})$  is the typical turnover time, and defining a dimensionless amplitude  $\xi = \delta/\delta_0$ , we arrive at the following Langevin equation for the LSC fluctuations  $\xi$

$$\dot{\xi} = \tilde{A} + \alpha \xi - \beta \xi^{3/2} + \tilde{f}_\xi(t), \quad (1)$$

with  $\tilde{A} = A\tau_\delta/\delta_0$ . Here the rescaled (dimensionless) diffusion coefficient is  $\tilde{D}_\delta \equiv D_\delta \tau_\delta/\delta_0^2$ , representing the amplitude of the scaled noise  $\tilde{f}_\xi(t)$ . We have included numerical prefactors  $\alpha, \beta = \mathcal{O}(1)$  to account for the geometric coefficients from the spatial volume averaging procedure. These constants will be determined below by demanding that the maximum and the width of the PDF are consistent with experimental results.

*Evolution of the azimuthal velocity:-* The equation for the horizontal motion is obtained from the Navier-Stokes equation for the azimuthal velocity,  $u_\theta \simeq L\dot{\theta}$ , by retaining the advection and momentum diffusion terms. Previously [12, 13], the viscous drag term was neglected on the basis that it is typically small. This approximation is valid in the regime of a well-defined LSC, but breaks down near cessations, since the momentum transport from the LSC also becomes very small. The viscous drag is dominant in the viscous boundary layer, so

that a spatial average along an arbitrary direction in the horizontal plane gives  $\langle \nu \nabla^2 \theta_0 \rangle \sim -\nu \theta_0/(L\lambda_\theta)$ . The viscous boundary layer thickness  $\lambda_\theta$  is estimated from balancing the advection force with the momentum diffusion force  $U\dot{\theta}_0/L \sim \nu \theta_0/\lambda_\theta^2$ ; together with the proportionality  $U/\tau_\delta \sim \alpha g \delta$ , we find that  $\lambda_\theta \sim \sqrt{\nu L \delta_0/(U_0 \delta)}$ . In addition to these deterministic forces, the self-advection term is mimicked by a delta-correlated Gaussian noise  $f_\theta(t)$  with amplitude  $D_\theta$ . Rescaling time by the typical time  $\tau_\theta \approx L^2/(\nu \text{Re})$  for crossing a boundary layer of thickness  $\lambda_\theta$  and  $\delta$  by  $\delta_0$ , the equation of motion for the azimuthal fluctuations is

$$\ddot{\theta}_0 = - \left( \alpha_1 \xi + \beta_1 \frac{\tau_\theta}{\tau_\delta} \sqrt{\xi} \right) \dot{\theta}_0 + \tilde{f}_\theta(t), \quad (2)$$

where the rescaled diffusion coefficient is  $\tilde{D}_\theta = D_\theta \tau_\theta$ , and  $\alpha_1, \beta_1 = \mathcal{O}(1)$  account for geometrical factors due to volume averaging. From the definition of the timescales,  $\tau_\theta/\tau_\delta = \text{Re}^{-1/2} \ll 1$  and hence the viscous drag term becomes important when  $\xi \ll (\beta_1/\alpha_1)^2 \text{Re}^{-1}$ , i.e. near cessations.

*Probability distribution for  $\delta$ :-* Since the Langevin equation for  $\xi$  is decoupled from that of  $\dot{\theta}$ , we first analyze Eq. (1) separately. In order to obtain the stationary PDF  $P(\xi)$  at long times, we use the equivalent Fokker-Planck equation of Eq. (1). It reads [14]

$$\frac{\partial P(\xi, t)}{\partial t} = - \frac{\partial}{\partial \xi} \left[ \left( \tilde{A} + \alpha \xi - \beta \xi^{3/2} \right) P(\xi, t) \right] + \frac{\tilde{D}_\delta}{2} \frac{\partial^2 P(\xi, t)}{\partial \xi^2}. \quad (3)$$

The stationary solution of this equation is

$$P(\xi) = C \exp[-2V(\xi)/\tilde{D}_\delta], \quad (4)$$

with

$$V(\xi) = -\tilde{A}\xi - \alpha \frac{\xi^2}{2} + \beta \frac{2}{5} \xi^{5/2}. \quad (5)$$

Note that Eq. (4) predicts that  $\log P(\xi \ll 1) \propto \xi$  as observed in experiment. Denoting the logarithmic derivative of the experimental PDF at small  $\xi$  by  $B$ , using (4) we find that  $\tilde{A} = B\tilde{D}_\delta/2$ . Here  $B$  and  $\tilde{D}_\delta$  are the tuning parameters of the theory and will be extracted from experimental data.

We now determine the constants  $\alpha$  and  $\beta$  by requiring that the PDF has a maximum at  $\xi = 1$  and width equal to  $\sqrt{\tilde{D}_\delta}$ , and fix the constant  $C$  by normalizing  $P(\xi)$  in its Gaussian regime close to  $\xi = 1$ . Expanding  $P(\xi)$  (4) in the vicinity of  $\xi = 1$  up to second order, we find that  $\tilde{A} + \alpha - \beta = 0$  for the maximum to be at  $\xi = 1$ , and  $(3/2)\beta - \alpha = 1/2$  for the variance to be  $\tilde{D}_\delta$ . This yields  $\alpha = 1 - 3\tilde{A}$  and  $\beta = 1 - 2\tilde{A}$ . With  $\tilde{A} = B\tilde{D}_\delta/2$ , the final normalized result for the PDF reads as

$$P(\xi) = \frac{1}{\sqrt{2\pi\tilde{D}_\delta}} e^{-3B/10 - 1/(5\tilde{D}_\delta)} \times e^{B\xi + \tilde{D}_\delta^{-1} [(1-3B\tilde{D}_\delta/2)\xi^2 - (4/5)(1-B\tilde{D}_\delta)\xi^{5/2}].} \quad (6)$$

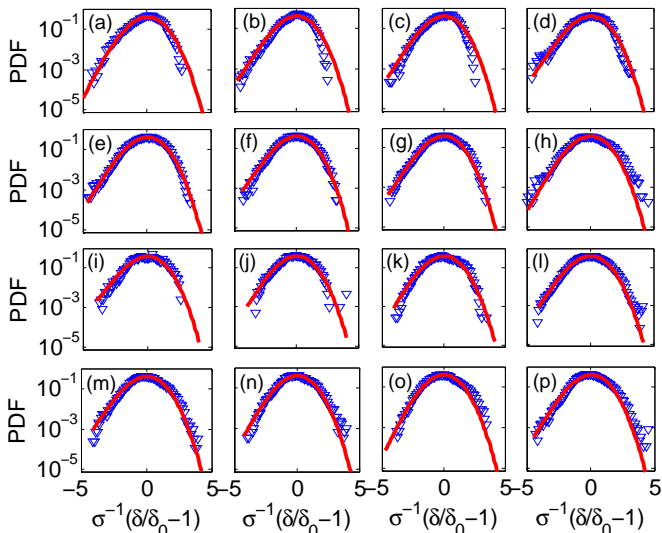


FIG. 1. (Color online) Theoretical (solid line) and experimental (triangles) PDFs for the normalized amplitude  $\xi$  versus  $(\xi - 1)/\sigma$  ( $\sigma = \sqrt{\tilde{D}_\delta}$ ), for different Ra numbers, with (a)-(h) for the medium sample and (i)-(p) for the large sample. The Ra numbers are:  $3.78 \cdot 10^8$  (a),  $8.16 \cdot 10^8$  (b),  $1.1 \cdot 10^9$  (c),  $2.3 \cdot 10^9$  (d),  $4.5 \cdot 10^9$  (e),  $7.9 \cdot 10^9$  (f),  $1.02 \cdot 10^{10}$  (g),  $1.51 \cdot 10^{10}$  (h),  $4.75 \cdot 10^9$  (i),  $7.16 \cdot 10^9$  (j),  $1.22 \cdot 10^{10}$  (k),  $2.43 \cdot 10^{10}$  (l),  $4.71 \cdot 10^{10}$  (m),  $5.68 \cdot 10^{10}$  (n),  $7.51 \cdot 10^{10}$  (o) and  $1.04 \cdot 10^{11}$  (p). In each subfigure the parameters  $\tilde{D}_\delta$  and  $B$  were computed by fitting the left tail of the experimental PDF to Eq. (7).

The only free parameters in this result are  $B$  and  $\tilde{D}_\delta$ . These are estimated from the  $\xi \ll 1$  asymptote of (6):

$$P(\xi \ll 1) \simeq (2\pi\tilde{D}_\delta)^{-1/2} e^{-3B/10-1/(5\tilde{D}_\delta)} e^{B\xi}. \quad (7)$$

By fitting the logarithm of the experimental PDFs to a line from the logarithm of Eq. (7), we extract  $B$  and  $\tilde{D}_\delta$  for each experimental data set. In Fig. 1 we show comparisons of experimental results and PDF (6) using the parameters  $B$  and  $\tilde{D}_\delta$  extracted from experimental results; very good agreement is evident for a wide range of Ra numbers. In this figure and henceforth the medium and large samples refer to cylindrical containers with heights 24.76cm and 50.61cm and aspect ratio of  $\sim 1$  [13].

Having calculated the complete PDF of the LSC amplitudes, we now extract the cessation frequency. The latter can be found by analyzing the following first-passage problem: starting from the vicinity of the fixed point  $\xi = 1$  what is the mean time it takes to reach the vicinity of  $\xi = \xi_0 \ll 1$ , where  $\xi_0 \ll 1$  is the amplitude which defines the experimental cessation threshold? Writing down the backward Fokker-Planck equation [14], the mean time to cessation (MTC) is given by

$$T(\xi, \xi_0) = 2 \int_{\xi_0}^{\xi} \frac{dy}{\psi(y)} \int_y^{\infty} \frac{\psi(z)}{\tilde{D}_\delta} dz; \quad \psi(z) = e^{-\frac{2[V(z)-V(\xi_0)]}{\tilde{D}_\delta}}, \quad (8)$$

where  $\xi \simeq 1$  is the effective initial condition, and the

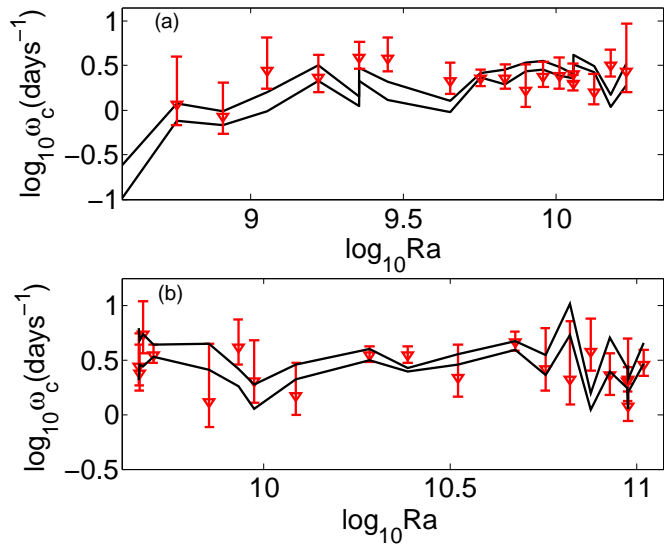


FIG. 2. (Color online) Cessation frequency (per day) as a function of Ra for the medium (a) and large (b) samples. Experimental results (triangles) [13] are compared to theoretical prediction (10). The latter are bound within the two solid lines. The experimental cessation was defined to occur when  $\delta/\delta_0 < \xi_{min}$ , that is, we have averaged over the time intervals between events where the system undergone cessation with  $\xi < \xi_{min}$ , see Eq. (10). Here,  $\xi_{min} = 0.15$  for the medium sample, and  $\xi_{min} = 0.2$  for the large sample. Similar results were obtained for thresholds of  $\xi_{min}$  between 0.15 and 0.3.

potential satisfies (5) with  $\tilde{A} = B\tilde{D}_\delta/2$ . Using the smallness of  $\tilde{D}_\delta$  (typically ranging between  $10^{-2}$ - $10^{-1}$ ), we can evaluate the inner integral by using the saddle point approximation. By doing so, we arrive at a result independent of  $y$ , which permits the evaluation of the outer integral using a Taylor expansion of the integrand about  $y = \xi_0$  [15]. This procedure leads to the final result for the MTC  $T_c(\xi_0)$  to reach a point  $\xi_0 \ll 1$  (see also [13]):

$$T_c(\xi_0) \simeq \frac{\tau_\delta \tilde{D}_\delta}{|V'(\xi_0)|} \sqrt{\frac{2\pi}{\tilde{D}_\delta}} e^{2\tilde{D}_\delta^{-1}[V(\xi_0)-V(1)]}, \quad (9)$$

where we have multiplied the result by  $\tau_\delta$  to present the time in physical units, and used the fact that  $V''(1) = 1/2$ . Given a threshold for cessation  $\xi_{min}$  as is done experimentally, in order to mimic the binning procedure of the experimental data, we have to average over  $\xi_0$  in Eq. (9) from 0 to  $\xi_{min}$ , which yields

$$\omega_c^{-1} \simeq \frac{1}{\xi_{min}} \int_0^{\xi_{min}} d\xi_0 T_c(\xi_0). \quad (10)$$

To obtain a theoretical prediction for  $\omega_c$  as a function of Ra, we use the extracted values of  $B$ ,  $\tilde{D}_\delta$  and  $\tau_\delta$  from the experimental data [13]. By doing so, we can plot the theoretical prediction for  $\omega_c$  as a function of Ra, as shown in Fig. 2. Here, the theoretical predictions (10) agree well with the experimental data [13], for both the medium and

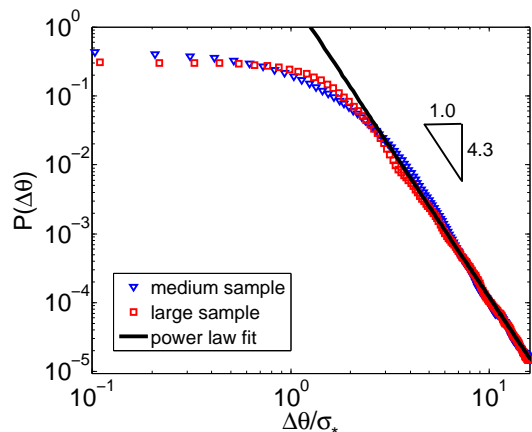


FIG. 3. (Color online) PDF  $P(\Delta\theta)$  averaged over all experimental PDFs with Ra numbers ranging from  $10^9$ - $10^{11}$  as a function of  $\Delta\theta/\sigma_*$ ;  $\sigma_*$  is a rescaling factor so that the medium (triangles) and large (squares) sample PDFs coincide at their right tail. The experimental data shown here was adaptively binned using the data threshold method [16] with threshold  $0.001 \max[P(\Delta\theta)]$ . Using the least-square method in the regime  $4 \lesssim \Delta\theta/\sigma_* \lesssim 20$ , the medium and large samples were found to scale with a power law of  $-4.34 \pm 0.02$  and  $-4.27 \pm 0.02$ , respectively, closely fitting the theoretical prediction of Eq. (13). The solid line is a power law of  $-4.3$ .

large samples. The error bars in the experimental results originate from the binning method, while the errors in the theoretical curves come from the uncertainties in the extracted values of  $B$  and  $\bar{D}_\delta$ .

*Probability distribution for  $\theta$ :* Now we turn to the calculation of  $P(\theta)$ . As the Langevin equation for  $\dot{\theta}$  [Eq. (2)] depends on  $\xi$ , for a given  $\xi$  we can first determine the steady state conditional PDF  $P(\dot{\theta}_0|\xi)$ . Using (2), we find

$$P(\dot{\theta}_0|\xi) = \frac{1}{\sqrt{2\pi\bar{D}_\theta}} e^{-(\alpha_1\xi + \beta_1\sqrt{\xi/\text{Re}})\dot{\theta}_0^2/\bar{D}_\theta}. \quad (11)$$

Given the PDF  $P(\xi)$  from Eq. (6), we then determine the complete PDF  $P(\dot{\theta}_0)$  of the azimuthal velocity by the following relation

$$P(\dot{\theta}_0) = \int_0^\infty d\xi P(\dot{\theta}_0|\xi)P(\xi), \quad (12)$$

which is valid when the relaxation timescale of  $\dot{\theta}$  is much faster than that of  $\delta$ , namely  $\tau_\delta \gg \tau_\theta$ . That is, Eq. (12) holds when the conditional PDF  $P(\dot{\theta}_0|\xi)$  equilibrates much faster than the typical timescale of change of  $\xi$ .

Integral (12) can be evaluated in the Gaussian regime of the PDF, where  $\xi \simeq 1$ , which yields the statistics of reorientations due to rotations of the LSC plane. In this case, to leading order one can simply put  $\xi = 1$  in Eq. (2) which gives  $P(\dot{\theta}_0) \sim e^{-\alpha_1\dot{\theta}_0^2/\bar{D}_\theta}$ . By comparing it with the experiments,  $\alpha_1 = 1$  in agreement with Ref. [13].

The cessation events correspond to the right hand tail of the PDF (12). Indeed, when the system undergoes

cessation and  $\xi \ll 1$ , the integrand is dominated by  $e^{-\beta_1\sqrt{\xi/\text{Re}}\dot{\theta}_0^2/\bar{D}_\theta}$ . Therefore, the right hand tail of the PDF given by Eq. (12) satisfies

$$P(\dot{\theta}_0) \sim \dot{\theta}_0^{-4}. \quad (13)$$

This power-law prediction for the tail of  $P(\dot{\theta}_0)$  is consistent with the earliest analysis of the experimental data [7, 12] (reporting an exponent of  $-3.8$ ), but differs from the numerical calculations presented in [12] which obtained a power-law with an exponent of  $-2$ . The difference arises as our equation of motion includes momentum diffusion that allows accurately accounting for the tail of  $P(\dot{\theta}_0)$ . In Fig. 3 we plot the experimental PDFs for  $\Delta\theta \sim \dot{\theta}$ , and show that they do indeed exhibit a power-law behavior at the tails with exponent of approximately  $-4.3$  in very good agreement with our prediction.

We thank Eric Brown and Guenter Ahlers for many helpful discussions and for generously sharing their data with us. M. A. gratefully acknowledges the Rothschild and Fulbright foundations for support. L. A. is grateful for support from the Center of Excellence for Physics of Geological Processes. This work was partially supported by the National Science Foundation through grant number NSF-DMR-1044901.

- 
- [1] R. Krishnamurti and L. Howard, Proc. Natl. Acad. Sci. USA **78**, 1981 (1981).
  - [2] E. Siggia, Annual Review of Fluid Mechanics **26**, 137 (1994).
  - [3] G. Ahlers, S. Grossmann, and D. Lohse, Reviews of Modern Physics **81**, 503 (2009).
  - [4] D. Funfschilling and G. Ahlers, Physical Review Letters **92**, 194502 (2004).
  - [5] H.-D. Xi, S.-Q. Zhou, Q. Zhou, T.-S. Chan, and K.-Q. Xia, Physical Review Letters **102**, 044503 (2009).
  - [6] E. Brown and G. Ahlers, J. Fluid Mech. **638**, 383 (2009).
  - [7] E. Brown and G. Ahlers, Journal of Fluid Mech. **568**, 351 (2006).
  - [8] E. van Doorn, B. Dhruva, K. Sreenivasan, and V. Cassella, Physics of Fluids **12**, 1529 (2000).
  - [9] J. Marshall and F. Schott, Reviews of Geophysics **37**, 1 (1999).
  - [10] P. Roberts and G. Glatzmaier, Reviews of Modern Physics **72**, 1081 (2000).
  - [11] M. Miesch and J. Toomre, Annual Review of Fluid Mechanics **41**, 317 (2009).
  - [12] E. Brown and G. Ahlers, Physical Review Letters **98**, 134501 (2007).
  - [13] E. Brown and G. Ahlers, Physics of Fluids **20**, 075101 (2008).
  - [14] C. W. Gardiner, *Handbook of Stochastic Methods* (Springer, Berlin, 2004).
  - [15] M. Assaf and B. Meerson, Physical Review Letters **97**, 200602 (2006).
  - [16] C. Adami and J. Chu, Physical Review E **66**, 011907 (2002).